Molecular Vision 2015; 21:316-323 <http://www.molvis.org/molvis/v21/316>
Received 25 July 2014 | Accepted 12 March 2015 | Published 15 March 2015

Lens capsule structure assessed with atomic force microscopy

Vivian M. Sueiras,[1] Vincent T. Moy,[2] Noël M. Ziebarth[1]

[1]Department of Biomedical Engineering, University of Miami College of Engineering, Coral Gables, FL; [2]Department of Physiology and Biophysics, University of Miami Miller School of Medicine, Miami, FL

Purpose: To image the ultrastructure of the anterior lens capsule at the nanoscale level using atomic force microscopy (AFM).

Methods: Experiments were performed on anterior lens capsules maintained in their in situ location surrounding the lens from six human cadavers (donor age range: 44–88 years), four cynomolgus monkeys (*Macaca fascicularis* age range: 4.83–8.92 years), and seven pigs (<6 months). Hydration of all samples was maintained using Dulbecco's Modified Eagle Medium (DMEM). Whole lenses were removed from the eye and placed anterior side up in agarose gel before gel hardening where only the posterior half of the lens was contained within the gel. After the gel hardened, the Petri dish was filled with DMEM until the point where the intact lens was fully submerged. AFM was used to image the anterior lens surface in contact mode. An integrated analysis program was used to calculate the interfibrillar spacing, fiber diameter, and surface roughness of the samples.

Results: The AFM images depict a highly ordered fibrous structure at the surface of the lens capsule in all three species. The interfibrillar spacing for the porcine, cynomolgus monkey, and human lens capsules was 0.68±0.25, 1.80±0.39, and 1.08±0.25 µm, respectively. In the primate, interfibrillar spacing significantly decreased linearly as a function of age. The fiber diameters ranged from 50 to 950 nm. Comparison of the root mean square (RMS) and average deviation demonstrate that the surface of the porcine lens capsule is the smoothest, and that the human and cynomolgus monkey capsules are significantly rougher.

Conclusions: AFM was successful in providing high-resolution images of the nanostructure of the lens capsule samples. Species-dependent differences were observed in the overall structure and surface roughness.

The lens capsule is an acellular basement membrane that completely encapsulates the lens of the eye. The capsule maintains the structural integrity of the lens material and serves as an anchorage point for the zonules [1]. The capsule, together with the ciliary muscles and zonules, alters the shape of the lens material during accommodation [1]. It separates the lens from other ocular tissues while protecting it from viruses and bacteria [2]. The capsule also functions as a medium of biochemical interchange [3]. It allows for the passive exchange of metabolic substrates and waste between the ocular environment and the lens cells, while selectively filtering molecules based on their size and charge [2,4]. Finally, interactions between the lens capsule and the lens epithelial and fiber cells are required for normal lens development and growth [5].

The molecular composition of the lens capsule is similar to other basement membranes throughout the body, although the lens capsule is the thickest basement membrane in the body due to the slow turnover rate and continuous deposition of matrix material [4,6,7]. The lens capsule is composed of networks of laminin [8-12], collagen IV [8,13,14], entactin/nidogen [8,9,15], and some heparin sulfate proteoglycans, including perlecan [8,16-18], collagen XVIII [19], collagen XV [20], and agrin [21]. Collagen type IV is the most abundant component [14], making up 30–40% of the lens capsule's dry weight [6]. Additional studies on the bovine lens capsule have shown a similar composition to that of the human [22]. The three-dimensional, interwoven networks of the various components of the lens capsule endow it with strength, flexibility, and elasticity, thus enabling the capsule to function successfully. Imaging studies have shown that this general network is the same in multiple mammalian species, including porcine, human, and ox [23].

Images of the ultrastructure of the anterior lens capsule surface have been previously acquired using cryoelectron microscopy [5,23], scanning helium ion microscopy [4], and atomic force microscopy (AFM) [24-27]. For cryoelectron microscopy and scanning helium ion microscopy techniques, irreversible modifications are made to the tissue when preparing it for imaging, such as freezing, fixation, sectioning, or critical point drying. With AFM, the tissue remains fully hydrated and intact up to and throughout the imaging process. However, these methods have not captured the three-dimensional ultrastructure of the fully hydrated lens capsule in its in situ location surrounding the lens

Correspondence to: Noël M. Ziebarth, Biomedical Atomic Force Microscopy Laboratory, Department of Biomedical Engineering, University of Miami College of Engineering, 1251 Memorial Drive, MEA 170A, Coral Gables, FL 33146; Phone: +1 (305) 284-4520; FAX: +1 (305) 284-6494; email: nziebarth@miami.edu

material. The purpose of the current study was to use AFM to image the structure of the fully hydrated lens capsule at the nanoscale level without excising the capsule from the lens.

METHODS

Tissue preparation protocol: Whole eyes were obtained from six human cadavers (donor age range: 44–88 years), four cynomolgus monkeys (*Macaca fascicularis* age range: 4.83–8.92 years), and seven pigs (<6 months; see Table 1). The donor human eyes were provided by the Florida Lions Eye Bank, the cynomolgus monkey eyes were provided by the Diabetic Research Institute and the Division of Veterinary Resources of the University of Miami, and the pig eyes were purchased from Visiontech (Sunnyvale, TX). The eyes arrived at the laboratory in sealed containers and were stored in the refrigerator at 4 °C before they were used. All human eyes were obtained and used in compliance with the guidelines of the Declaration of Helsinki for research involving the use of human tissue. The animal eyes were obtained after enucleation following approved institutional animal care guidelines. All animal experiments adhered to the ARVO Statement for the Use of Animals in Research.

The lens is situated behind the cornea and iris; therefore, these two structures must be removed before the lens can be isolated from the whole eye globe. The cornea was excised by making a small incision with a scalpel in the sclera, which is just lateral to the cornea. Ophthalmic surgical scissors were then used to cut around the cornea, detaching it from the eye entirely. With this approach, the iris usually remains affixed to the cornea during its removal. The lens is suspended in the eye by zonules (the suspensory ligament of the lens) extending from the rim of the lens to the ciliary body. The lens was separated by sectioning the zonules with a scalpel and placed in Dulbecco's Modified Eagle's Medium (DMEM, D1145, Sigma-Aldrich, St. Louis, MO) until it could be further prepared for imaging.

To stabilize the lens for AFM imaging, the posterior half was embedded in a liquid solution of 5% agarose gel (1.25 g agarose/25 ml deionized water, A0169–100G, Sigma-Aldrich, St. Louis, MO). The lens was inserted in the agarose gel after it had cooled to room temperature, to the point where it was nearly solidified. After the gel hardened, the exposed portion of the embedded lens was fully submerged in DMEM to prevent dehydration. It is important to note that the time between embedding the lens and experimentation was minimized to decrease the osmotic effects that the agarose gel may inflict on the lens. Additional studies should investigate alternate methods of preparing the agarose solution in an isotonic buffer to avoid possible changes to lens shape and stresses on the capsule. The anterior pole of the lens, corresponding to the anterior lens capsule, was imaged with an atomic force microscope (MFP-3D-BIO AFM, Asylum Research, Santa Barbara, CA) equipped with leg extenders specifically designed for the MFP-3D system. The leg extenders allow the AFM system to accommodate the embedded lens in its entirety without compromising the integrity of the images captured.

Imaging with the atomic force microscope: High-magnification images of all lens capsule samples were obtained in contact mode, in which the cantilever tip is held in constant contact with the sample surface, maintaining constant cantilever deflection while scanning. The piezoelectric mechanism (Z piezo) applies vertical position corrections to keep this deflection constant, thus mapping the actual three-dimensional topography of the sample surface. Although intermittent contact (AC) mode imaging has lower lateral drag forces that may damage the sample, contact mode was selected so that the full range of the Z piezo would be available for extension and/or retraction of the cantilever to compensate for the lens's curvature. A pyramidal, silicon nitride AFM cantilever tip (20 nm tip radius, nominal spring constant 0.01 N/m, MLCT series, Bruker AFM Probes, Camarillo, CA) was used to image all samples. All samples were fully submerged in DMEM throughout the imaging. Therefore, the AFM cantilever tip was also in fluid during imaging. The AFM tip was visually positioned above the central pole of the anterior surface, so all images were within approximately 1 mm from the center. Height and deflection images were acquired for all samples at multiple scan lengths (1.15 µm x 1.15 µm to 40 µm x 40 µm) using the MFP-3D AFM system software (Asylum Research, Santa Barbara, CA), based in IGOR Pro (WaveMetrics, Lake Oswego, OR).

Table 1. The age, postmortem time, and sample size for all lens capsules imaged in this study.

Species	Sample size	Age range (years)	Postmortem time (days)
Human	6	44 - 88	2–16
Cynomolgus monkey	4	4.83 – 8.92	3–8
Pig	7	<6 months	2–7

Image post-processing: All height data used to reconstruct the images were obtained from the Z-sensor signal channel rather than the direct height signal. The height data collected from the height signal is not accurate when sample features are greater than 0.1 µm because piezoelectric materials exhibit a mechanical hysteresis, responding nonlinearly to voltage. Since the Z-sensor signal is obtained from the linear variable differential transformer (LVDT) position sensors attached to the piezo stacks, this signal corresponds to the true topography of the sample surface.

All Z-sensor images obtained were processed using AR software (Igor Pro, Wavemetrics, Portland, OR) integrated with the MFP-3D-BIO AFM. To compensate for the natural curvature of the lens capsule in situ, all data were flattened using an x-y plane fit as well as a flatten order 1. A 3×1 median filter was also applied to the images. The edges of the scan, where the piezoelectric actuator was out of range of the sample height (pure white or pure black image), were not included in the analysis. Care was also taken to minimize the inclusion of motion artifacts common at the end of image acquisition (at the bottom of the image). The post-processed data were used to generate height and three-dimensional images.

Image analysis: After post-processing, all images were analyzed with the AR software included with the Asylum AFM. The height data were extracted for one representative line of data for each image. The interfibrillar spacing was calculated by finding the peak-to-peak distances along this line of data using OriginLab software. The fiber dimensions were calculated as the full width at half maximum of the peaks along the line of data. Only the smallest scan sizes available for each sample were used to determine the fiber dimensions, since the scans represented the finest resolution. Four quantitative parameters were used to characterize the roughness of the lens capsule surface: root-mean-square (RMS) deviation, average deviation, skewness (asymmetry around the mean), and kurtosis (peakedness or flatness compared to the normal distribution). These values were calculated for each Z-sensor image. Any images with motion or adhesion artifacts were excluded from the roughness analysis.

RESULTS

The height and three-dimensional images obtained from the Z-sensor signal after post-processing are shown in Figure 1. These images depict the vertical displacement of the cantilever tip as it is scanned across the topography of the sample. The images show a highly ordered fibrous structure at the surface of the lens capsule in all three species. This organization was expected, since the lens capsule is comprised predominately of fibrous proteins (collagen IV and laminin) networked with entactin/nidogen and perlecan, forming the meshwork seen in Figure 1. The white lines (areas of higher topography) correspond to fibers whereas the darker gray and black areas correspond to openings in the mesh.

The interfibrillar spacing for the porcine, cynomolgus monkey, and human lens capsules was 0.68±0.25, 1.80±0.39, and 1.08±0.25 µm, respectively (Table 2). The spacing was significantly different among the porcine, monkey, and human lens capsules (p=0.002 and p=0.008, respectively). The spacing of the human and monkey lens capsules was also significantly different (p=0.01). However, the human and non-human primate data were grouped together using a scaling factor of 1 monkey year to 3 human years [28-30] to determine if age was the reason for the statistical difference. This analysis showed that interfibrillar spacing significantly decreased linearly as a function of age in the primate (p=0.028).

The fiber diameters for the porcine, cynomolgus monkey, and human lens capsules were 306 nm±239 nm (range: 50 nm–950 nm), 397 nm±159 nm (range: 176 nm–687 nm), and 339 nm±135 nm (range: 67 nm–691 nm), respectively (Table 2). There were no statistical differences between the fiber diameters in any of the three species (p=0.235 for porcine–cynomolgus, p=0.381 for porcine–human, p=0.286 for cynomolgus–human). There was also no relationship between fiber diameter and age for the primate (p=0.529).

The roughness parameters for the three species are summarized in Table 2. Comparison of the RMS and average deviation demonstrate that the surface of the porcine lens capsule is the smoothest, and that the human and cynomolgus monkey capsules are significantly rougher (p=0.057 and 0.040, respectively, for RMS deviation; 0.058 and 0.046, respectively, for average deviation). The roughness of the human and monkey lens capsules are comparable (p=0.171 and 0.188 for RMS deviation and average deviation, respectively). No significant relationship was found with age for the human and monkey lens capsules, although there was a trend toward decreasing surface roughness with age. Kurtosis values indicate that the human lens capsules have the most gradual transitions from high to low area topographies.

DISCUSSION

Prior investigations into the structure of the lens capsule used cryoelectron microscopy and helium ion microscopy, and therefore required extensive tissue preparation before imaging. A few additional studies used atomic force microscopy to image the surface of the lens capsule, but the experiments were performed on excised samples. In the current

study, images of the lens capsule, in its native, unprocessed state, were captured. Furthermore, AFM allowed the lens capsule to be maintained in a hydrated state throughout the imaging process, mitigating time-sensitive morphological changes that occur ex vivo. Finally, the current study expanded upon previous AFM studies by imaging the lens capsule in its in situ location surrounding the lens material.

The fibrous network at the surface of the lens capsule was observed in all three of the species imaged in this study: humans, cynomolgus monkeys, and pigs. The images clearly show that the porcine lens capsule had the most densely packed structure, whereas the cynomolgus monkey had clearly defined openings or pores. The structure of the human lens capsule was intermediate, with some porous areas surrounded by a densely interwoven fibrous structure. Previous studies investigating anterior lens capsule mechanical properties [30] and thickness [31] found no statistical differences between cynomolgus monkeys and humans for either of these two parameters. Since the mechanical properties of tissues are directly correlated to the organization of the individual components [32-34], it is reasonable that the lens capsule structure would also be comparable for humans and

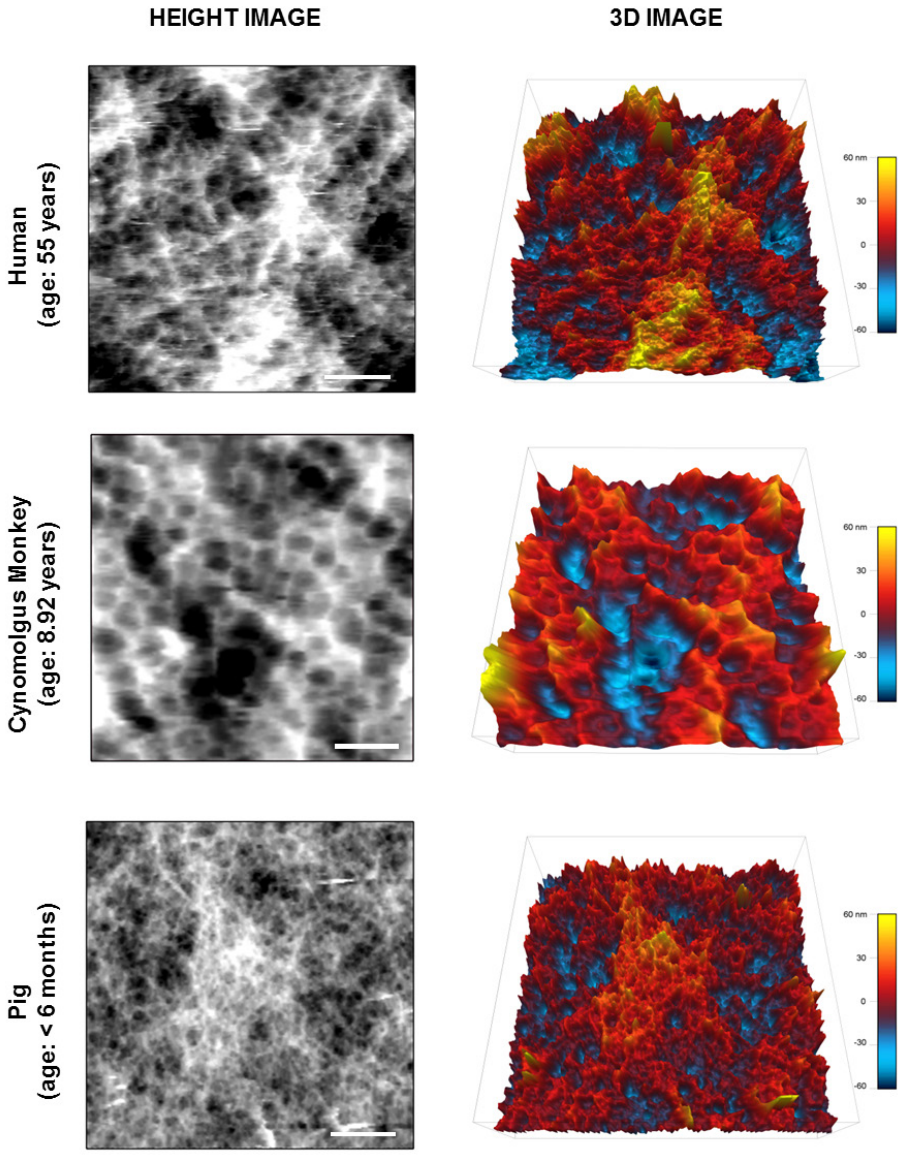

Figure 1. Representative height and 3D images obtained on the lens capsule for human, cynomolgus monkey, and pig. The grayscale corresponds to 70 nm in height. The scale bar represents 2 µm. In the 3D image, the color scale corresponds to 120 nm.

cynomolgus monkeys. For the porcine lens capsule, a study by Danielsen [35] found that the capsule is approximately four times thicker but 50% less stiff than the human lens capsule. Therefore, these differences in thickness and mechanical properties should be manifested in differences in structure as well, as shown in this study (see Figure 1). Interestingly, the fiber diameters were not significantly different among the species. This suggests that the actual network comprises the same components, but the organization of these components with varying interfibrillar spacing and additional layers to increase thickness endows the lens capsule with different mechanical properties seen in previous studies. Furthermore, the pig lens is unable to accommodate [36]. Since the lens capsule distributes the forces of accommodation on the lens material during accommodation [37], the organizational layout of the collagen network may be different in species that accommodate versus those that do not.

The structural differences seen in this study could be explained by differences in age. The age range of the human capsules was 44–88 years, whereas the cynomolgus monkeys ranged from 14 to 17 equivalent human years, using a conversion factor of 1 monkey year equal to 3 human years [28-30]. When the human and cynomolgus interfiber spacing was analyzed together, a significant decrease was found with age. Although the data support the theory that interfibrillary spacing has a direct correlation with the primate's age, additional interspecies differences, independent of age, might have influenced the results. For example, compositional variations in the lens capsule between species could have affected the imaged structure; however, the absence of previous studies of additional species in the literature makes it difficult to draw any further conclusions.

Previous studies investigating the lens capsule ultrastructure showed a similar fibrous structure as seen in the current study [23-27,38]. Atomic force microscopy images of the excised lens capsule showed fiber-like surface structures [24-27] with diameters ranging from 1 to 100 nm wide [26,27], which is at the low end of the range found in the current study. In a classic study, Barnard et al. used cryoelectron microscopy [23] and observed images of a highly ordered collagen IV matrix, with interfibrillar spaces measuring 30 nm. In another study, Danysh et al. used helium ion microscopy and observed pore-like structures measuring 6–25 nm at the surface of the anterior lens capsule [38]. The current study found interfibrillar spaces on the order of 1 µm. Although differences in the technique used could result in differences in the dimensions, it is most likely that the AFM images in the current study captured a larger-scale view of the lens capsule surface than those in previous studies. It is possible that imaging at higher magnification would provide more details about a structure within the structures observed in this study. Nevertheless, the current study provides insight into the lens capsule structure in three different species.

During AFM scans, the piezoelectric mechanism makes vertical adjustments to keep the force applied to the sample constant, which provides information on the sample height. The surface roughness can be calculated from these vertical displacements of the cantilever with subnanometer precision. Analysis of the roughness data (RMS roughness and average deviation) showed that the surface of the porcine lens capsules was significantly smoother than that of cynomolgus monkeys or humans. This could be because the fibrous structure is so dense in porcine lenses, with very small pore-like openings (pure black area in the image). The height differences measured go from a higher fiber to a lower fiber, as opposed to an opening in the structure, as was seen in the cynomolgus monkey and human lens capsules (see Figure 1). The RMS roughness values found in the current study for humans (12–58 nm) are comparable to those found in a previous AFM investigation by Creasey et al. on excised anterior lens capsules (5–50 nm) [26]. An additional AFM study by Choi et al. [25] found that anterior lens capsules from patients with cataract were less rough than those from non-cataract patients. Interestingly, our results for the human lenses showed a decreasing trend in roughness with age, although this was not statistically significant due to the small range in age (44–88 years). The degree of cataract progression in the lenses included in the current study was not noted,

Table 2. Summary of structural and roughness parameters for the three species.

Species	Interfibrillar spacing (µm)	Fiber diameter (nm)	RMS deviation (nm)	Average deviation (nm)	Skewness (no unit)	Kurtosis (no unit)
Pig	0.68±0.25	306±239	12.74±1.12	10.06±0.88	0.20±0.27	1.30±0.97
Cynomolgus monkey	1.80±0.39	397±159	37.96±19.40	29.54±16.00	0.21±0.61	2.31±2.14
Human	1.08±0.25	339±135	25.72±16.62	20.28±13.13	−0.02±0.05	0.47±0.61

The values provided are the average ± standard deviation of all images included in the analysis.

so a correlation with cataract, as in the Choi et al. study, could not be made. A larger value for roughness could indicate that the samples were deteriorating as a function of sample postmortem time. However, the postmortem time of the monkey samples was comparable to that of the porcine samples, but the monkey samples were significantly rougher.

With AFM, we image and analyze the outer topography of the lens capsule. Because of the continuous deposition of the capsule by the fiber cells and the lens epithelium lining the anterior capsule's posterior surface [2], the outer layer of the lens capsule would have been formed during the early stages of the organism's development. For the specific species investigated in this study, the fibrous networks of the anterior lens capsule imaged in the porcine lenses were formed months before the AFM imaging whereas the outer layer of the primate lens capsules were formed years to decades before the AFM imaging. Such ample time leaves the possibility for protein oxidation to occur [39,40], possibly affecting the roughness and structure of the lens capsule's outer layer. In addition, pigs are unable to accommodate [36]. Therefore, the porcine lens capsule is not subjected to the continual mechanical stresses throughout its lifetime to which the lens capsule of a primate is accustomed [37]. It is possible that mechanical stress correlates to the surface roughness at the nanoscale. In fact, this study found an increase in roughness with increasing amplitude of accommodation (porcine, human, monkey).

All images of the lens capsule were obtained in contact mode operation of the AFM. Contact mode has been criticized because it can create lateral drag forces between the cantilever tip and the sample's surface that may actually damage the sample. However, selecting a slower scan rate can minimize these lateral forces and the occurrence of sample damage and drag artifacts. To further mitigate possible damage to the sample from the cantilever, the set point, corresponding to the cantilever's vertical force on the sample, was kept below 1.875 V (approximately 5 nN). Adjustments to the set point also helped compensate for changes to the tissue postmortem, including water diffusion into the lens that causes lens capsule delamination. A previous study looked at lens biometry while immersed in various preservation media, including DMEM [41]. This study found that monkey and human lenses swelled less than 10% after 5 h in the solution. Therefore, although the network would expand correspondingly, we anticipate the changes would be small.

In summary, atomic force microscopy was used to successfully image the fully hydrated lens capsule. Species-dependent differences were observed in the overall structure and surface roughness. Further studies should investigate structure as a function of age to determine how the lens capsule changes with increased age in different species.

ACKNOWLEDGMENTS

Monkey eyes were provided by the Diabetic Research Institute and the Division of Veterinary Resources of the University of Miami. Donor human eyes were provided by the Florida Lions Eye Bank. This research was supported by the American Federation for Aging Research (AFAR) Research Grant and NSF MRI 0722372.

REFERENCES

1. Courtois Y. The Capsule of the Crystalline Lens. In: Obrecht LSaG, editor. Presbyopia: Recent research and reviews from the third international symposium: Professional Press Books/ Fairchild Publications Division of Capital Cities Media, Inc.; 1987.
2. Danysh BP. The lens capsule. Exp Eye Res 2009; 88:151-64. [PMID: 18773892].
3. Fisher RF. The structure and function of basement membrane (lens capsule) in relation to diabetes and cataract. Trans Ophthalmol Soc U K 1985; 104:755-9. [PMID: 3868215].
4. Danysh BP. Characterizing molecular diffusion in the lens capsule. Matrix Biol 2010; 29:228-36. [PMID: 20026402].
5. Danysh BP, Duncan MK. The lens capsule. Exp Eye Res 2009; 88:151-64. [PMID: 18773892].
6. Marshall GE, Konstas AG, Bechrakis NE, Lee WR. An immunoelectron microscope study of the aged human lens capsule. Exp Eye Res 1992; 54:393-401. [PMID: 1521568].
7. Burd HJ. A structural constitutive model for the human lens capsule. Biomech Model Mechanobiol 2009; 8:217-31. [PMID: 18622755].
8. Cammarata PR, Cantu-Crouch D, Oakford L, Morrill A. Macromolecular organization of bovine lens capsule. Tissue Cell 1986; 18:83-97. [PMID: 3515629].
9. Cammarata PR, Spiro RG. Identification of noncollagenous components of calf lens capsule: evaluation of their adhesion-promoting activity. J Cell Physiol 1985; 125:393-402. [PMID: 3905828].
10. Kohno T, Sorgente N, Ishibashi T, Goodnight R, Ryan SJ. Immunofluorescent studies of fibronectin and laminin in the human eye. Invest Ophthalmol Vis Sci 1987; 28:506-14. [PMID: 3549611].
11. Muraoka M, Hayashi T. Three polypeptides with distinct biochemical properties are major alpha chain-size components of type IV collagen in bovine lens capsule. J Biochem 1993; 114:358-62. [PMID: 8282726].
12. Parmigiani C, McAvoy J. Localisation of laminin and fibronectin during rat lens morphogenesis. Differentiation 1984; 28:53-61. [PMID: 6394411].

13. Brinker JM, Pegg MT, Howard PS, Kefalides NA. Immunochemical characterization of type IV procollagen from anterior lens capsule. Coll Relat Res 1985; 5:233-44. [PMID: 2412754].

14. Kelley PB, Sado Y, Duncan MK. Collagen IV in the developing lens capsule. Matrix Biol 2002; 21:415-23. [PMID: 12225806].

15. Dong L, Chen Y, Lewis M, Hsieh JC, Reing J, Chaillet JR, Howell CY, Melhem M, Inoue S, Kuszak JR, DeGeest K, Chung AE. Neurologic defects and selective disruption of basement membranes in mice lacking entactin-1/nidogen-1. Lab Invest 2002; 82:1617-30. [PMID: 12480912].

16. Laurent M, Lonchampt MO, Regnault F, Tassin J, Courtois Y. Biochemical, ultrastructural and immunological study of in vitro production of collagen by bovine lens epithelial cells in culture. Exp Cell Res 1978; 115:127-42. [PMID: 210028].

17. Rossi M, Morita H, Sormunen R, Airenne S, Kreivi M, Wang L, Fukai N, Olsen BR, Tryggvason K, Soininen R. Heparan sulfate chains of perlecan are indispensable in the lens capsule but not in the kidney. EMBO J 2003; 22:236-45. [PMID: 12514129].

18. Peterson PE, Pow CS, Wilson DB, Hendrickx AG. Localisation of glycoproteins and glycosaminoglycans during early eye development in the macaque. J Anat 1995; 186:31-42. [PMID: 7649817].

19. Fukai N, Eklund L, Marneros AG, Oh SP, Keene DR, Tamarkin L, Niemela M, Ilves M, Li E, Pihlajaniemi T, Olsen BR. Lack of collagen XVIII/endostatin results in eye abnormalities. EMBO J 2002; 21:1535-44. [PMID: 11927538].

20. Ylikärppä R, Eklund L, Sormunen R, Muona A, Fukai N, Olsen BR, Pihlajaniemi T. Double knockout mice reveal a lack of major functional compensation between collagens XV and XVIII. Matrix Biol 2003; 22:443-8. [PMID: 14614990].

21. Fuerst PG, Rauch SM, Burgess RW. Defects in eye development in transgenic mice overexpressing the heparan sulfate proteoglycan agrin. Dev Biol 2007; 303:165-80. [PMID: 17196957].

22. Cammarata PR, Cantu-Crouch D, Oakford L, Morrill A. Macromolecular organization of bovine lens capsule. Tissue Cell 1986; 18:83-97. [PMID: 3515629].

23. Barnard K, Burgess SA, Carter DA, Woolley DM. Three-dimensional structure of type IV collagen in the mammalian lens capsule. J Struct Biol 1992; 108:6-13. [PMID: 1562433].

24. Doudevski I, Rostagno A, Cowman M, Liebmann J, Ritch R, Ghiso J. Clusterin and complement activation in exfoliation glaucoma. Invest Ophthalmol Vis Sci 2014; 55:2491-9. [PMID: 24550356].

25. Choi S, Lee HJ, Cheong Y, Shin JH, Jin KH, Park HK, Park YG. AFM study for morphological characteristics and biomechanical properties of human cataract anterior lens capsules. Scanning 2012; 34:247-56. [PMID: 22331648].

26. Creasey R, Sharma S, Craig JE, Gibson CT, Ebner A, Hinterdorfer P, Voelcker NH. Detecting protein aggregates on untreated human tissue samples by atomic force microscopy recognition imaging. Biophys J 2010; 99:1660-7. [PMID: 20816080].

27. Tsaousis KT, Karagiannidis PG, Kopsachilis N, Symeonidis C, Tsinopoulos IT, Karagkiozaki V, Lamprogiannis LP, Logothetidis S. Measurements of elastic modulus for human anterior lens capsule with atomic force microscopy: the effect of loading force. Int Ophthalmol 2014; 34:519-23. [PMID: 24037592].

28. Qiao-Grider Y, Hung LF, Kee CS, Ramamirtham R, Smith EL 3rd. Normal ocular development in young rhesus monkeys (Macaca mulatta). Vision Res 2007; 47:1424-44. [PMID: 17416396].

29. Bito LZ, DeRousseau CJ, Kaufman PL, Bito JW. Age-dependent loss of accommodative amplitude in rhesus monkeys: an animal model for presbyopia. Invest Ophthalmol Vis Sci 1982; 23:23-31. [PMID: 7085219].

30. Ziebarth NM, Arrieta E, Feuer WJ, Moy VT, Manns F, Parel J-M. Primate lens capsule elasticity assessed using Atomic Force Microscopy. Exp Eye Res 2011; 92:490-4. [PMID: 21420953].

31. Ziebarth NM, Manns F, Uhlhorn SR, Venkatraman AS, Parel JM. Noncontact optical measurement of lens capsule thickness in human, monkey, and rabbit postmortem eyes. Invest Ophthalmol Vis Sci 2005; 46:1690-7. [PMID: 15851570].

32. Rho JY, Kuhn-Spearing L, Zioupos P. Mechanical properties and the hierarchical structure of bone. Med Eng Phys 1998; 20:92-102. [PMID: 9679227].

33. Bull HB. An Introduction to Physical Biochemistry. Philadelphia, PA: FA Davis Company; 1971.

34. Intrigila B, Melatti I, Tofani A, Macchiarelli G. Computational models of myocardial endomysial collagen arrangement. Comput Methods Programs Biomed 2007; 86:232-44. [PMID: 17451838].

35. Danielsen CC. Tensile mechanical and creep properties of Descemet's membrane and lens capsule. Exp Eye Res 2004; 79:343-50. [PMID: 15336496].

36. Kuszak JR, Mazurkiewicz M, Jison L, Madurski A, Ngando A, Zoltoski RK. Quantitative analysis of animal model lens anatomy: accommodative range is related to fiber structure and organization. Vet Ophthalmol 2006; 9:266-80. [PMID: 16939454].

37. Krag S, Andreassen TT. Mechanical properties of the human lens capsule. Prog Retin Eye Res 2003; 22:749-67. [PMID: 14575723].

38. Danysh BP, Patel TP, Czymmek KJ, Edwards DA, Wang L, Pande J, Duncan MK. Characterizing molecular diffusion in the lens capsule. Matrix Biol 2010; 29:228-36. [PMID: 20026402].

39. Truscott RJ. Age-related nuclear cataract-oxidation is the key. Exp Eye Res 2005; 80:709-25. [PMID: 15862178].

40. Varma SD, Chand D, Sharma YR, Kuck JF Jr, Richards RD. Oxidative stress on lens and cataract formation: role of light and oxygen. Curr Eye Res 1984; 3:35-57. [PMID: 6360540].

41. Augusteyn RC, Rosen AM, Borja D, Ziebarth NM, Parel JM. Biometry of primate lenses during immersion in preservation media. Mol Vis 2006; 12:740-7. [PMID: 16865087].